
Diane Rivet, diane.rivet@geoazur.unice.fr
Université de la Côte d'Azur, Observatoire de la Côte d'Azur, CNRS, IRD, Géoazur

Benoit de Cacqueray
Thales Defense Mission System

Anthony Sladen
Université de la Côte d'Azur, Observatoire de la Côte d'Azur, CNRS, IRD, Géoazur

Aurélien Roques
Lycée Jules Ferry

Gaëtan Calbris
FEBUS-optics

Preliminary assessment of shipping noise monitoring using Distributed Acoustic Sensing on an optical fiber telecom cable

Diane Rivet[1,a], Benoit de Cacqueray[2], Anthony Sladen[1], Aurélien Roques[3], Gaëtan Calbris[4]

[1] *Université de la Côte d'Azur, Observatoire de la Côte d'Azur, CNRS, IRD, Géoazur*

250 route d'Albert Einstein, 06220 Valbonne, France

[2] *Thales Defense Mission System, 525 Route des Dolines, 06560 Valbonne, France*

[3] Lycée Jules Ferry, 06400 Cannes, France

[4] *FEBUS-optics, Technopole Helioparc, 2 av. Président Pierre Angot , 64 000 Pau, France*

[a] diane.rivet@geoazur.unice.fr

Abstract

Distributed acoustic sensing (DAS) is a recent instrumental approach allowing to turn fiber-optic cables into dense arrays of acoustic sensors. This technology is attractive in marine environments where instrumentation is difficult to implement. A promising application is the monitoring of environmental and anthropic noise, leveraging existing telecommunication cables on the seafloor. We assess the ability of DAS to monitor such noise using a 41.5 km-long cable offshore Toulon, France, focusing on a known and localized source. We analyze the noise emitted by the same tanker cruising above the cable, first 5.8 km offshore in 85 m deep bathymetry, and then 20 km offshore, where the seafloor is at a depth of 2000 m. The spectral analysis, the Doppler shift, and the apparent velocity of the acoustic waves striking the fiber allow us to separate the ship radiated noise from other noise. At 85 m water depth, the signal to noise ratio is high and the trajectory of the boat is recovered with beamforming analysis. At 2000 m water depth, although the acoustic signal of the ship is more attenuated, signals below 50 Hz are detected. These results confirm the potential of DAS applied to seafloor cables for remote monitoring of acoustic noise even at intermediate depth.

I. Introduction

Ambient noise in the ocean results from natural and anthropogenic sources. The anthropogenic noise produced by maritime traffic has increased dramatically with the development of industrialization and global trading (Frisk 2012). Over the last decade, the scientific community has shown that it strongly impacts all of marine fauna, from mammals to zooplankton, including fish, sea turtles, and invertebrates (e.g. Williams et al. 2015, Mustonen et al. 2020). For example, marine mammals use sound for vital activities such as finding food, detecting predators, breeding, and navigation. There is now a strong awareness in the community of a need to limit man-made underwater noise, and international efforts have led to legislation at regional and international levels to limit the impact on marine ecosystems (Merchant 2019).

Automatic Identification System (AIS) data provide unique identification, position and trajectories of vessels. From the type, size and speed of the ship reported in AIS, the radiated noise source level can be compared with measurements (Wales and Heitmeyer, 2011, McKenna et al. 2012) or predicted using shipping noise models (e.g. Wales and Heitmeyer, 2002) but oceanographic conditions, as well as ship design, can strongly modify the radiated noise (e.g. McKenna et al. 2013). Furthermore, AIS is self-declarative and only involves large vessels (Vespe et al. 2012). Yet in coastal areas~~,~~ small vessels without AIS, such as recreational ships, can generate significantly more noise than AIS vessels (Hermannsen, et al. 2019). Independent monitoring of ships is also crucial for key infrastructures such as harbors, power plants and for safety and security aspects. For instance, submarine telecom cables which are very sensitive for global communications can be damaged by anchors, seabed trawlers, and other types of activities (Rønnekleiv et al. 2019). Therefore, to better evaluate environmental and anthropic noise~~-~~sources and their impacts on marine species, continuous monitoring of acoustic noise, both on the coast and offshore, needs to be done.

Passive acoustic instruments developed to study anthropic and natural underwater noise, such as HARPs (high-frequency acoustic recording packages), can be deployed from boats anywhere (Wiggins and Hildebrand 2017). This instrumentation provides broad band 10 Hz to 160 kHz omnidirectional acoustic measurements for an extended period of time (up to 300 days). Ocean Bottom Seismometers (OBS) often include a hydrophone and can provide low frequency (<400Hz) acoustical records up to four years ~~for~~ using long-term autonomous platforms such as MUG-OBS (Hello et al., 2019). However, though these acoustic instruments can be deployed anywhere, they do not allow data to be transmitted in real time. Other solutions outside academia like SOSUS (Sound Surveillance System) with horizontal arrays moored ~~in~~ on the seafloor can provide real-time sound measurements but with very restricted access to scientists (Nishimura & Conlon, 1994). Overall, measuring acoustic noise over long distances continuously and for an extended period of time with conventional passive acoustic instruments requires expensive installation and maintenance.

Distributed Acoustic Sensing (DAS) on existing seafloor optical cables provides remote monitoring of the acoustic noise over several tens of kilometers offshore at relatively low cost but the feasibility of monitoring acoustic waves in all oceanic domains and bandwidths remains to be assessed. Measuring acoustic noise over several tens of kilometers from the shore enables real time monitoring. However, DAS delivers huge data volumes (a terabyte per day) and relevant on-the-fly processing to ensure real-time monitoring of acoustic noise is not yet available.

DAS measures both elastic and acoustic waves striking optical fibers. This technology has the potential to strongly impact many scientific domains and, in recent years, there has been a growing interest in applications in the earth and environmental sciences. DAS exploits changes in the light that is backscattered from random nano defects in the optical fiber to sense passing acoustic or seismic waves. These external mechanical waves induce a longitudinal strain of the fiber which can be related to a linear phase shift of the Rayleigh backscattered light. The strain or strain-rate is measured from the phase changes over a distance~~-~~called the gauge length, and thus corresponds to the integration of the strain or strain-rate along the gauge length. Figure 1 describes the principle of DAS acquisition and instrumental setup and in Appendix A we express the strain and strain rate measured by DAS for acoustic waves striking the fiber. In seismology, seismic waves are generally measured with a gauge length of about ten meters (e.g. Jousset el al. 2018, Ajo-Franklin et al. 2019).

DAS has proved to be efficient for monitoring sensitive infrastructures such as pipelines, railways, dams, and is becoming more and more common in seismic imaging and in the monitoring of oil fields and wells (e.g. Mateeva et al. 2013, Miller et al. 2016, Lellouch et al., 2019). Terrestrial seismology applications use either dedicated optical fiber cables dug in the soil (e.g. Daley et al. 2013; Feigl et al. 2019) or telecom dark fiber (eg. Dou et al. 2017; Yu et al., 2019). Academic DAS applications in the underwater environment started in 2019 (Sladen et al. 2019, Lindsey et al. 2019, Williams et al., 2019) with numerous observations -small local seismicity, large teleseismic earthquakes, surface gravity waves, microseismic noise- all with unprecedented spatial resolution. However, these studies focused on the low-frequency content of the DAS measurements, and the true potential of the approach at higher frequency than those used in seismology ($f > 20$ Hz) still needs to be explored and quantified. Under shallow water depth conditions (30m), Rønnekleiv et al. (2019) demonstrated the potential of DAS to detect and distinguish boats and trawlers. The drawbacks of DAS versus hydrophones are related to a more limited bandwidth at high frequency (the acquisition rate is controlled by the length of the fiber – the light pulse has to travel back and forth before the next pulse is emitted) and a cosine square angular sensitivity that renders DAS blind to signals arriving from a direction closely perpendicular to that of the optical fiber cable (Mateeva et al. 2014). Some progress has been made to counteract this last point through helically wound fibers that recover energy from all directions (e.g. Hornman 2014, Kuvshinov 2016). However, these limitations are in some way mitigated by the dense sampling in space of the waves hitting the fiber. This high resolution in space leads to an improvement in the signal-to-noise (SNR) ratio by simple summation of the strain rate observations and in the recovery of the azimuth and position of the acoustic sources through beamforming. Here, we further explore the potential of the technology to monitor and recognize anthropic acoustic noise sources using a well-identified and localized source of acoustic noise both in ~~a~~ shallow and deep water.

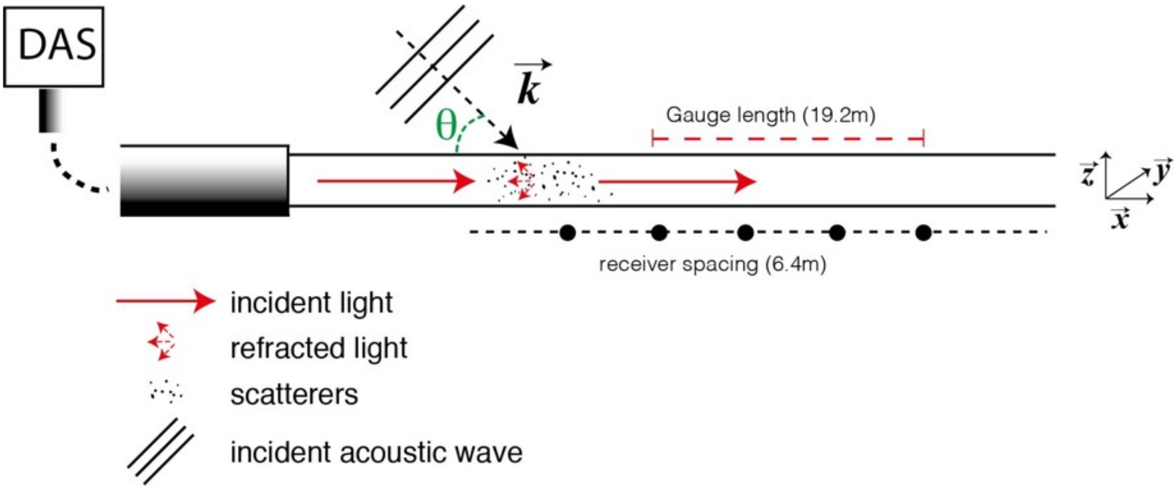

Figure 1 DAS acquisition principle and spatial sensing setup. The DAS acquisition unit is sending a light pulse inside a dark optical fiber. Along the path, the laser pulse interacts with the molecular-scale random scatters inherently present in all telecom fibers. The phase of the refracted light is analyzed for a set of virtual receivers regularly spaced, here 6.4m. The phase difference is analyzed over a gauge length of 19.2m to derive the strain-rate variations over that segment.

II. Method and instrumental setup

The DAS acquisitions were made on a 41.5 km-long electro-optic telecommunication cable from Alcatel deployed offshore Toulon in the south of France. The MEUST- NUMerEnv project (Mediterranean Eurocentre for Underwater Sciences and Technologies - Neutrino Mer Environnement, Lamare 2016) is operating the cable and provides power and data transmission for numerous oceanographic studies in the framework of the EMSO program (European Multidisciplinary Seafloor Observatory, Favali & Beranzoli, 2009) and for the

KM3NeT/ORCA (Oscillation Research with Cosmics in the Abyss) neutrino detector (Coyle et al. 2017). Crossing different oceanic domains of the Mediterranean margin, from the continental shelf to the abyssal plain, the cable, which is simply resting on the seafloor, reaches a depth of 2400 m on the abyssal plain (Figure 2). From 2.1km up to 17.2 km off the coast, the cable armoring is Single Armoring Heavy (SAH) then Light-Weight Protection (LWP) for the remaining 24 km.

The DAS interrogator, provided by Febus Optics, was used from February 19th to February 24th, 2018. In this experiment, the gauge length was fixed to 19.2 m with a spatial sampling of 6.4 meters (figure 1).

With a temporal sampling of 2kHz, waves up to 1kHz can be accurately retrieved with no temporal aliasing. With this configuration, DAS covers the low frequency range of hydrophones. When processing DAS as an array of receivers using beamforming and f-k representation, we should also consider the maximum frequency for non-spatially aliased signals. The Nyquist frequency f_N is related to the apparent wave velocity and the spatial sampling Δx through the relation $f_N = c/(2cos(\theta)\Delta x)$ with c the velocity and θ the bearing angle. For acoustic waves traveling parallel to the fiber cable (for a bearing of 0 or 180°) and having a velocity in seawater of 1500m/s, the spatial sampling allows to record a non-spatially aliased acoustic signals up to 117 Hz. Above this frequency false sources can appear in beamform analysis.

Large vessels report their position to the Automatic Identification System (AIS) database. This allowed us to identify that during the DAS acquisition, an 85m long tanker passed twice over the fiber-optic cable, first 5.8 km offshore with a N260° route at a velocity of 11 knots and, a few days later, the same tanker passed over the cable at 20km from the coast with a N83° route at a velocity of 7.8 knots, crossing the fiber at an angle of 71° (Figure 2, red bars).

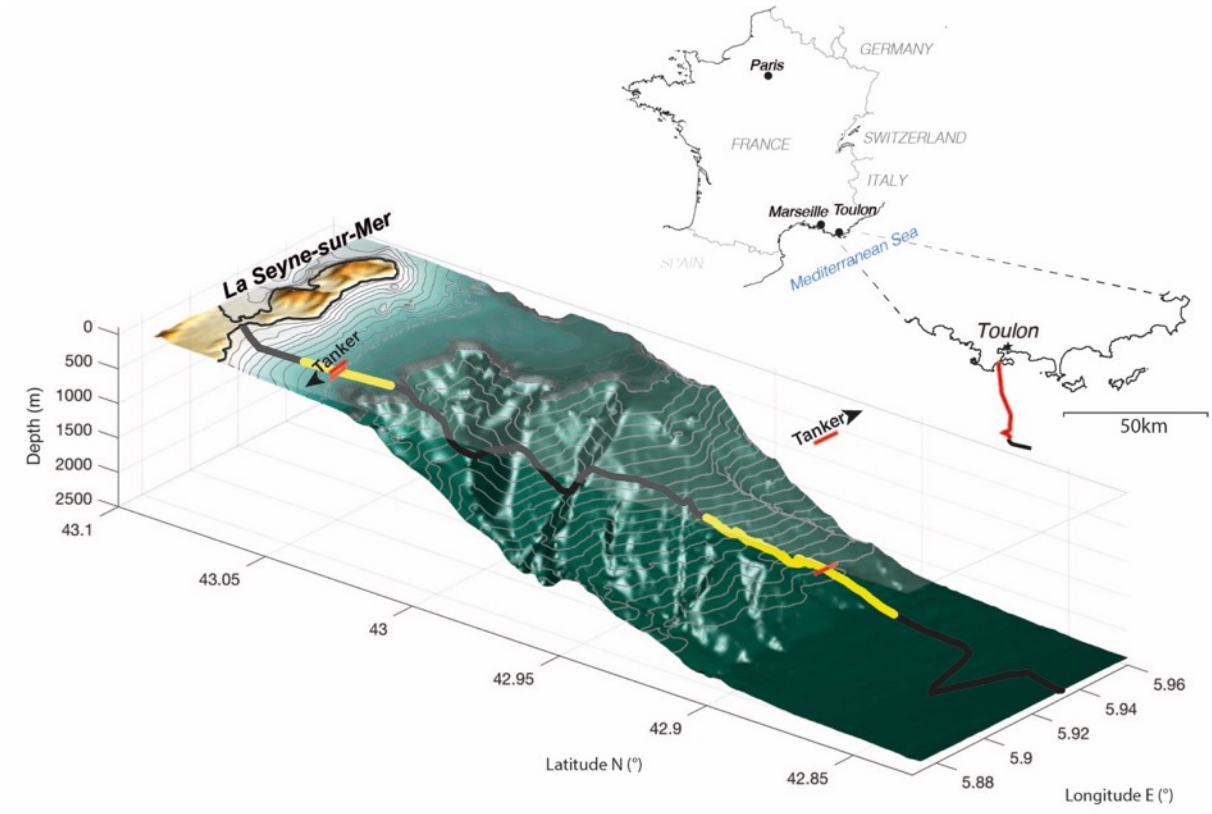

Figure 2 *(color online) Location of the MEUST-Numerenv optical fiber offshore of La Seyne-sur-Mer located in the vicinity of Toulon, south of France. The 41.5 km cable lies on the continental shelf for the first 7.5 kilometers before reaching the steep continental slope. The first 35 km of the cable is indicated by the red section of the cable indicated in the map. The first route of the tanker at 5,8 km from the coast and the second route at 20 km from the coast, known from the AIS GPS positions, are shown by the red thick line on the sea surface. The projection of the tanker routes crossing the cable at 5.8 and 20 km are indicated by the red lines on the sea floor. The two yellow sections of the cable indicate the portion of the fiber we used to detect the acoustic waves emitted by the ship.*

III. Maritime vessel noise detection

There is already a long history of studies modeling radiated ship noise (e.g. Gray and Greeley 1980). The variety of potential noise sources and their interactions makes the topic complex to summarize (Fournier 2009). However, a constant feature of ship radiated noise is a spectrum characterized by two main components (e.g. Pillon 2016). The first one is a signal resulting from multiple sources like cavitation, pumps, fans, fluid flowing in the pipes or along the shell. This component is sometimes considered having a Gaussian shape with a maximum at a few dozens of Hertz. The second component is a sum of narrow band signals coming from rotating elements (mainly linked to propeller activity but not only) and electrical wires (50 or 60 Hz). Frequencies higher than 1kHz are also characterized by narrow band signals, often with a noise floor showing a decreasing slope of several dB per decade.

At 85m depth, strain-rate records on the fiber show both features of ship radiated noise: the Fourier transform of 8 minutes of signals coming from one DAS receiver shows high amplitude narrow band signals (Figure 3). The intensity recorded by the DAS system in this experiment is uncalibrated, therefore we express the power relative to the maximum energy received from the passing boat. These narrow bands signals, with high signal to noise ratio, appear in the strain-rate time-frequency diagram, as the boat approaches the fiber (Figure 3a). At its dominant frequency, around 49Hz, the power of the boat radiated noise, averaged over an interval of 9 minutes, is 18 dB/Hz higher than the environmental and instrumental noise (Figure 3a). Considering the mean ship velocity given by the AIS system during this period (about 11 knots) and its route (almost perpendicularly to the fiber), it means that the 49Hz signal from the ship is recorded over 1700m. And if the boat displacement is roughly symmetric across the fiber, it means that the signal starts to be detected about 850m away from the fiber (Figure 4). On the strain rate time series, the ship radiated noise level increases by a factor of two in a time window of one minute (Figure 3b).

At 2000m depth, the acoustic noise emitted from the boat is more attenuated and the signal to noise ratio is lower (Figure 5). Hardly any significant increase of the amplitude of strain-rate time series is observed when the tanker passes over the cable. Still, after time-spectral analysis, we identify narrow bands with high energy and some at the same frequency as those observed at shallow depth. At its dominant frequency, 49Hz, the power of the spectral line reaches 8dB/Hz higher than noise on average during the 9 minutes of records. Another line around 57Hz is still visible. However, spectral lines around 16Hz, 33Hz, 41Hz, 76Hz and 83Hz observed on the first day at shallow depth are not visible. This can be caused by changes in the tanker speed, heterogeneous ground coupling along the cable , as well as the greater attenuation of the acoustic waves in a the 2000m water column. Besides, at higher depth, wave propagation can be affected by the velocity profile of the water column so that some rays can be refracted without reaching the bottom. Nevertheless, at short range, the propagation is mainly top-down so that bottom reflection can occur even if the sub-surface velocity differs from the water velocity. Using a constant velocity gradient of 0.016 m.s-1 commonly used for Mediterranean sea bellow 200m (e.g. Salon et al. 2003) we found that the different paths that reach the bottom at 2000 m depth are almost straight up to 8 km away from a surface source. See Figure S1 for the ray tracing model.

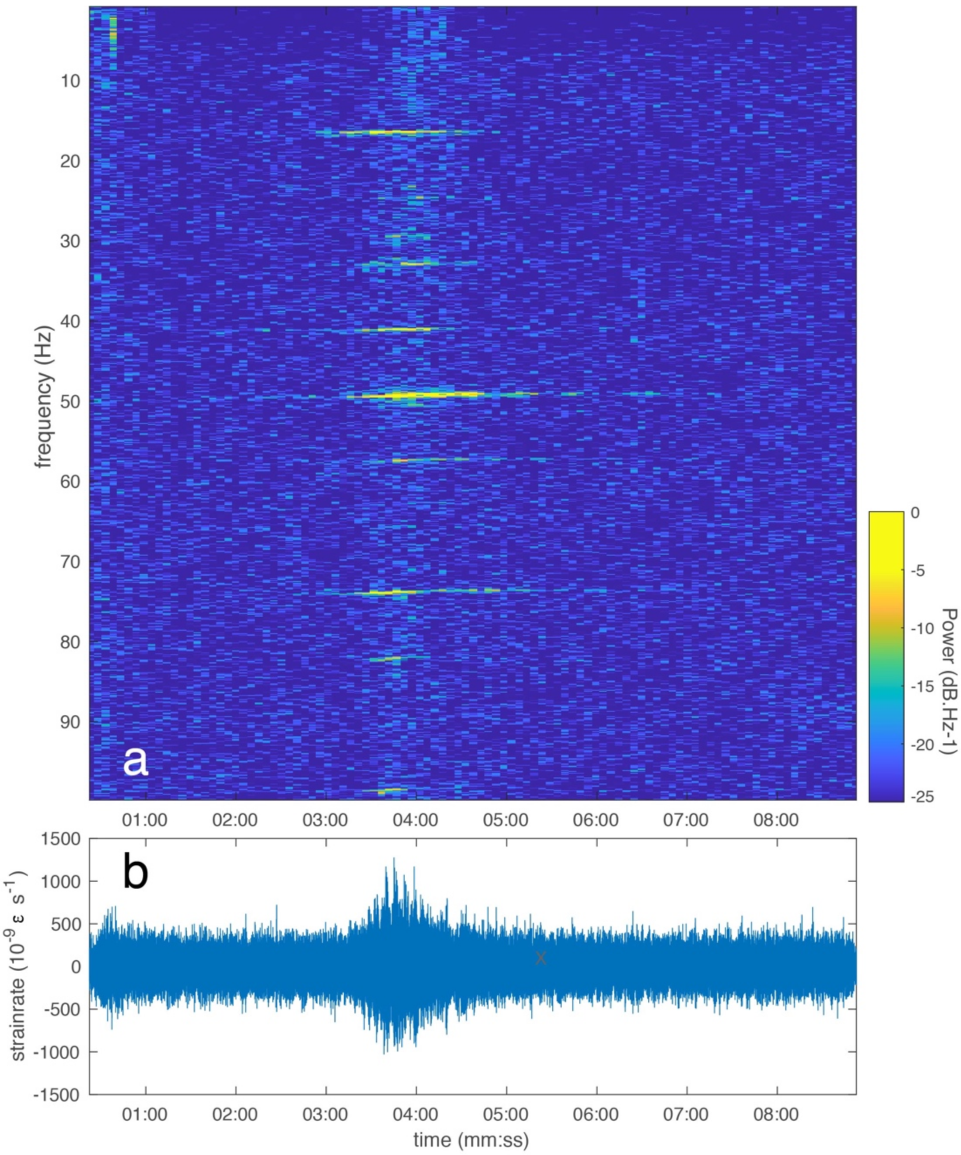

Figure 3 *(color online) Analysis of the temporal and spectral radiated noise of the tanker when passing above the optical fiber section 5.8km from the shore and 85m deep. (a) Power spectrogram density of the recorded strain-rate measured on the fiber at 5.651 km from the shore between 0 and 100Hz relative to the maximum power of* $20 \times 10^{-6} \varepsilon^{2}\ s^{-2}$ *at the dominant frequency 49Hz, (b) the corresponding time series.*

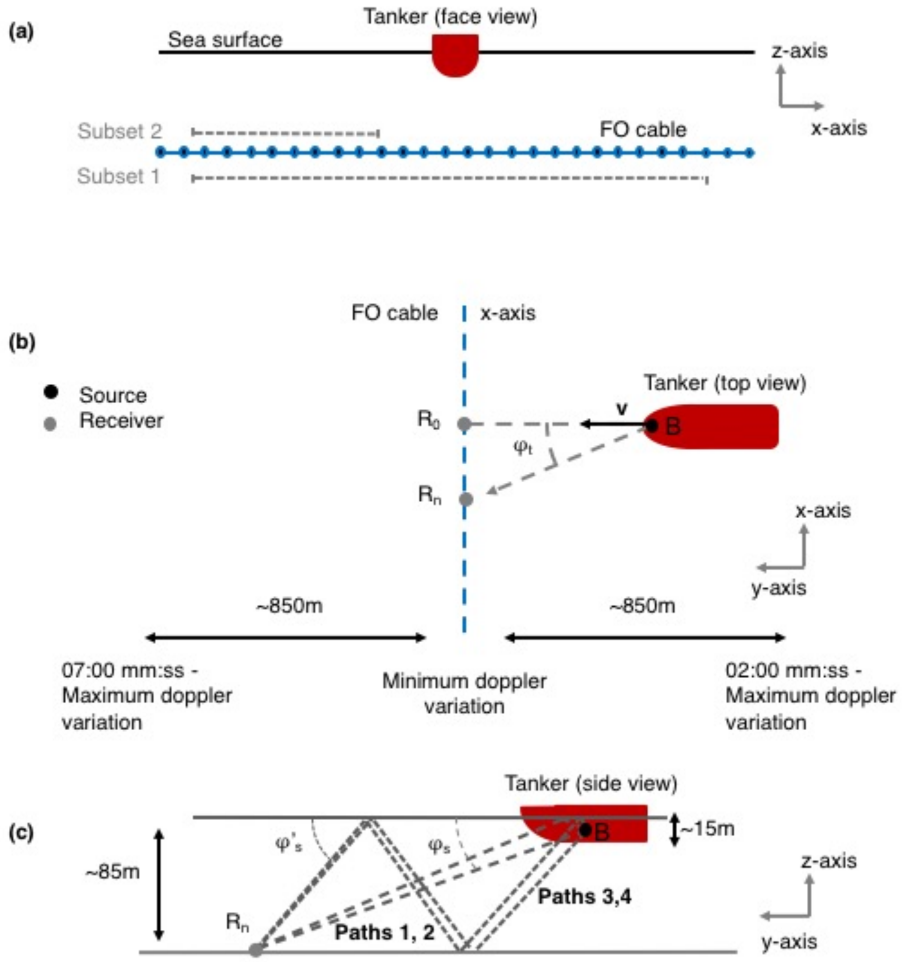

Figure 4 *Ship displacement (a) face, (b) top and (c) side views. The trajectory of the tanker B is described by the velocity vector* **v**. *R_0 is the closest receiver to the axis of the tanker and R_n indicates another receiver on the fiber optic cable. Ray paths are shown by dashed lines (assuming that ray approximation is valid, i.e. for high enough frequencies). Angles φ_t and φ_s are respectively the projections on the horizontal plane xBy and on the vertical plane yBz of the angle φ between the boat trajectory and the direct path from the boat to the receiver R_n.*

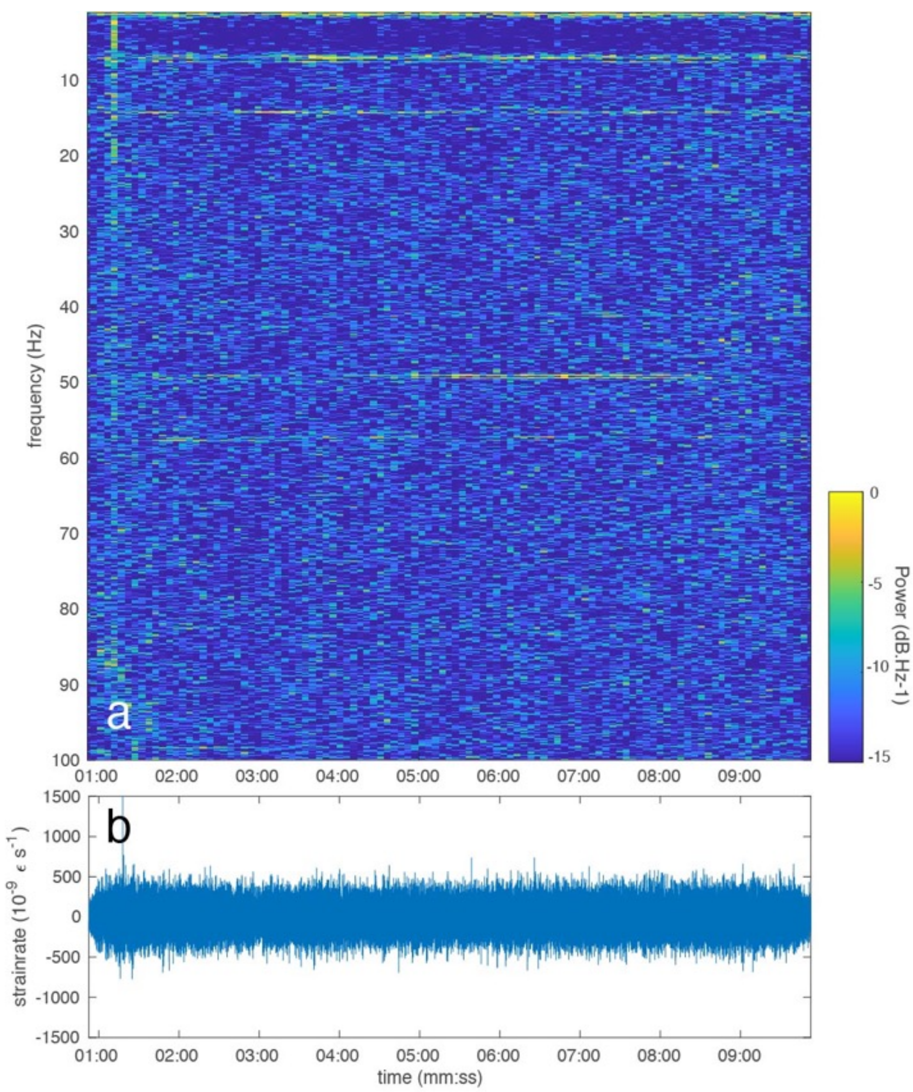

Figure 5 *(color online) Analysis of the temporal and spectral radiated noise of the tanker when passing above the optical fiber section 20 km from the shore and 2000m deep. (a) Power spectrogram of the recorded strain-rate measured on the fiber at 19.494 km from the shore between 0 and 100Hz relative to the maximum power of* $6.7\times 10^{-6}\varepsilon^{2}\, s^{-2}$ *at the dominant frequency 49Hz (b) the corresponding time series.*

By computing short Fourier transforms every 4 seconds for each receiver in the vicinity of the ship, we monitor in space and time the power of spectral lines radiated by the ship as it travels above the fiber at 85m (Figure 6). We observe that the distance range at which we can detect the tanker changes as a function of the frequency. Both the signal power and the attenuation of acoustic waves depend on the frequency and therefore control the distance over which we detect a signal. Another important feature are ring-like high-power patterns, clearly visible at 41Hz, 49Hz and 57Hz, related to the interference of acoustic waves reflected from the surface and the sea bottom (see Section IV). At 17Hz, the ring-like pattern is not visible probably because the wavelength at this frequency equals the water layer thickness and is controlled by a modal propagation. Using MOCTESUMA (a coupled normal-mode model, Etter 2003, 2012) and taking into account four layers in the bottom, we found that 17 modes can propagate with this frequency and at this channel depth.

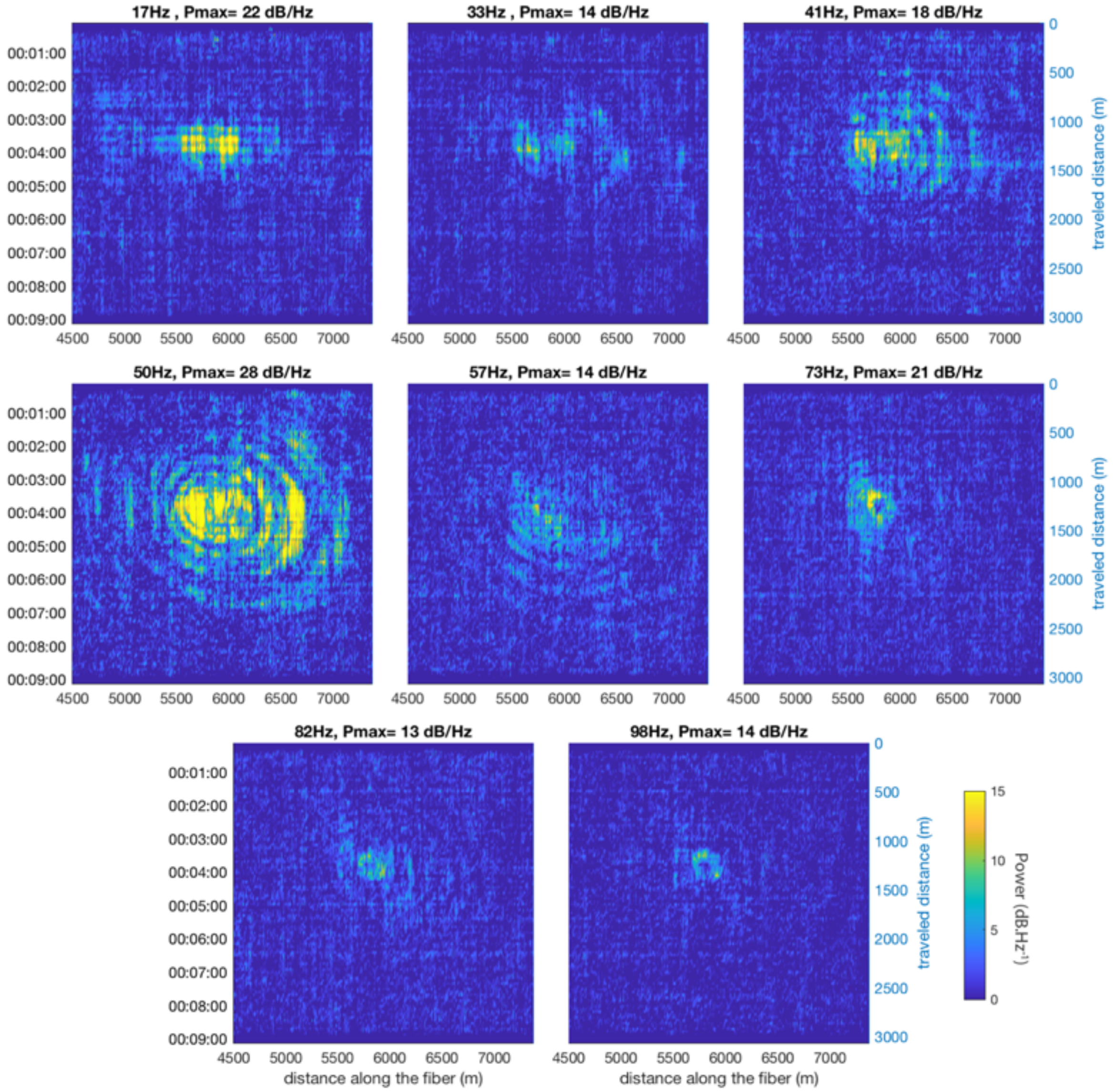

__Figure 6__ (color online) Acoustic noise power of the spectral lines radiated by the ship in time and space when passing above a section of fiber-optic cable 85m deep. The distance traveled by the boat and the time of the measurement are indicated on the right and left sides of the figures, respectively. The distance traveled by the boat is estimated from its velocity of 11 knots. On each figure, the title indicates the central frequency of the analysis in a 1Hz narrow band, as well as the maximum recorded power relative to instrumental and environmental noise measured at $191 \times 10^{-9}\varepsilon^2\ s^{-2}$ *in the [17 100]Hz frequency band. Note that the distance along the fiber is measured from the shore.*

We perform the same type of analysis for the tanker when it is cruising above a 2000m deep section of the fiber-optic cable (Figure 7). Because of the more complex bathymetry, it is harder to track the accurate position of the tanker from these maps. However, high power at different frequencies between 4 and 6 minutes and between 20 and 21 kilometers indicates a position of the boat close to the fiber and consistent with AIS records.

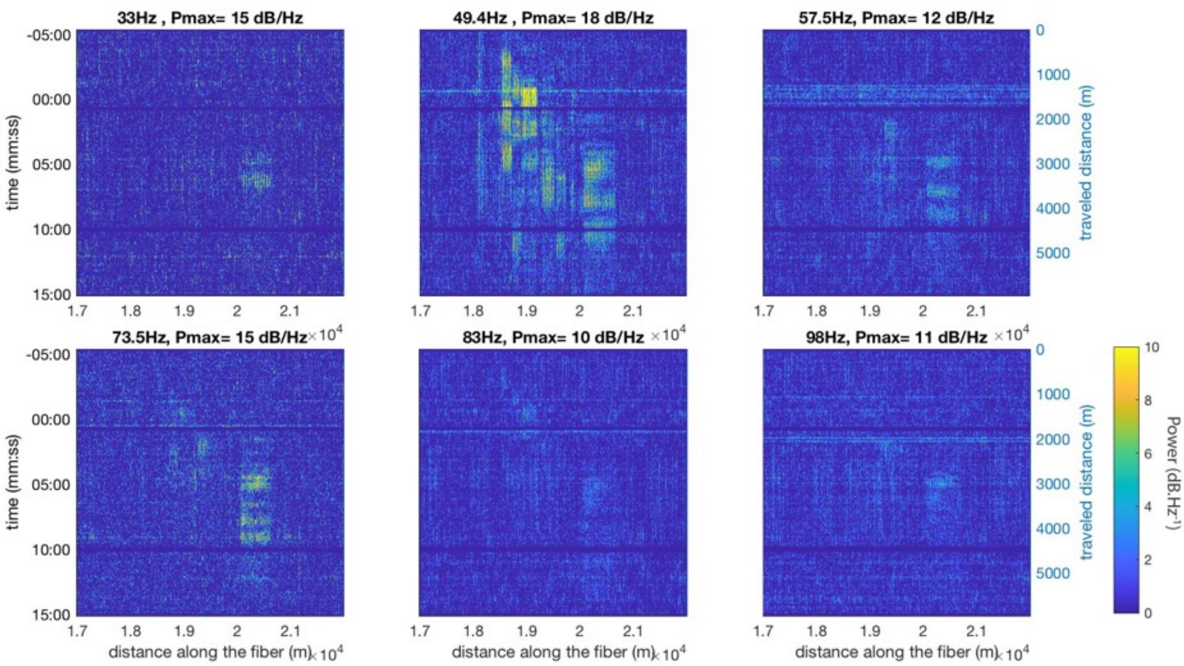

***Figure** 7 (color online) Acoustic noise power of the spectral lines radiated by the ship in time and space when passing above a section of fiber-optic cable 2 000m deep. The distance and time traveled by the boat are indicated on the right and left sides of the figures respectively. The distance traveled by the boat is derived from its velocity of 7,8 knots. On each figure, the title indicates the central frequency of the analysis in a 1Hz narrow band, as well as the maximum recorded power as well as the maximum recorded power relative to instrumental and environmental noise measured at* $206 \times 10^{-9}\varepsilon^2\ s^{-2}$ *in the [17 100]Hz frequency band. Note that the distance along the fiber is measured from the shore.*

IV Optical fiber cable response to an acoustic point source

We model the intensity of the wavefield in time and space for an acoustic point source using plane waves following ray trajectories. We convert the acoustic wave into the longitudinal strain-rate, and compute-the fiber optic response for the specified gauge length.

We express the strain and strain rate for acoustic waves reaching the fiber and sensed by DAS in an iso-speed water profile, following the same approach as proposed by Bakku (2015) for P-waves (Appendix A). For an incoming acoustic wave with particle velocity A_v, angular frequency ω, wavenumber $\vec{k}$ and propagation velocity c, the corresponding strain induced along the x axis of the fiber can be written as:

$$\varepsilon_{xx} = \frac{-A_v}{c} cos^2\theta e^{i(\omega t - \vec{k}.\vec{r})} \qquad \textbf{\textit{(1)}}$$

where θ is the angle between $\vec{k}$ and the x axis, and $\vec{r}$ the vector between the source and the receiver, ω the pulsation and t the time. The DAS measures strain-rate averaged over the gauge length L, leading to the following response:

$$\dot{\varepsilon}_{DAS} = \dot{\varepsilon}_{xx} sinc\left(k_x \frac{L}{2}\right) \qquad \textbf{\textit{(2)}}$$

This is equivalent to the difference in particle velocities on the x axis component of two geophones separated by L (Mateeva et al 2014).

Assuming the source is located at 15m depth, taking into account the tanker draft, eight acoustic rays have been used to predict the radiated sound field (see Figure 4). Adding more paths did not change the intensity maps. Path 1 runs from the source directly to each receiver. Path 2 has approximately the same path but hits the surface first. Both paths are represented by dashed lines in Figure 4b. Other paths are deduced by adding one, two, or more bottom-surface reflection sequences to paths 1 and 2. For example, paths 3 and 4 are represented in dashed lines in Figure 4b. The reflection coefficient depends on the incident angle - the Fresnel coefficient is computed and applied for each reflection - and on the nature of the soil, mainly composed by shales (Mascle 1971, Appendix B). In a 90m depth water channel and using wavefield modal description, Turgut et al. 2010 showed interferences of acoustic waves reflected on the sea surface for a source located at a depth down to $\lambda/4$. With a source at 15m, for frequencies higher than 25Hz, such interferences should be measured on the seafloor.

The intensity maps have been simulated over 4 minutes of record for the 2, 4, and 8 first paths at 49.4Hz (Figure 8a,b,c). Figure 4 shows paths 1 to 4. Paths 5 to 8 are the other four are the next two multiples. In Figure 8a, we observe a symmetric shape with intensity reaching zero when k_x equals zero, due to the null response of the fiber in the direction perpendicular to the cable (broadside). The figure has only two lobes of high intensity as we only model the direct path of the acoustic waves. In Figure 8b, which includes 4 paths, we observe a kind of ring shape that becomes more obvious in Figure 8c with 8 paths modeled. The comparison of Figures 7a,b,c allows us to understand the origin of the ring shape we observe in the real data (Figure 5). Due to the ship's motion over the fiber, the multipath interferences are permanently varying and create ring shapes on the 49.4Hz response.

The shape of the 8-paths model prediction is not exactly the same as the one recorded on the fiber (Figure 8d). Many reasons can explain this discrepancy: varying coupling of the fiber, varying depth for the considered area and possible fiber curvature. Besides, for the recorded data, we could not separate the two emitted frequencies close to 49.5 Hz in the intensity maps. Nevertheless, the size and spacing of the ring-like shapes are similar enough so that the signals recorded by the fiber appear to come from acoustic multipath interfering within the water channel. Underwater telecom cables, therefore, also behave as seismometers recording elastic signals coming from the ground (e.g. Sladen et al. 2019) and pressure waves from inside the water layer.

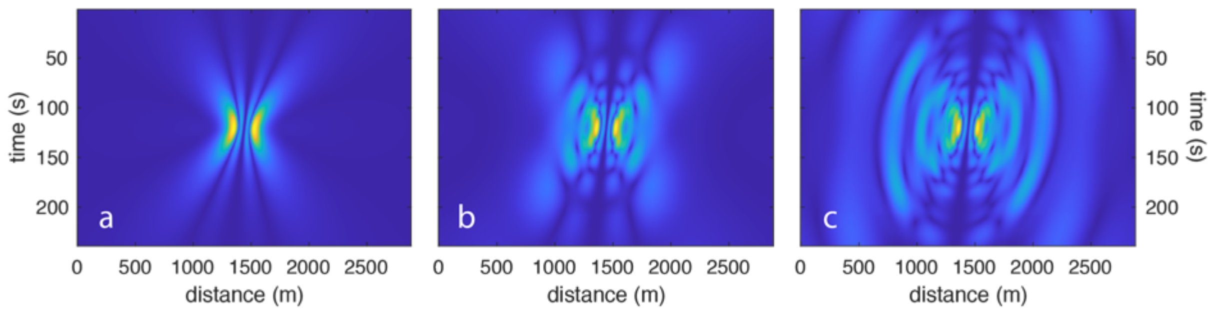

Figure 8 *(color online) Simulated signal intensity recorded by a fiber-optic cable, 85m deep, for a 49.4Hz source at the surface moving almost perpendicular to the fiber (80-degree bearing) with a constant velocity of 11 knots. From left to right, the subset figures correspond to simulations acknowledging more reverberations: (a) 2 paths, (b) 4 paths, and (c) 8 paths (see Figure 4b for a schematic description). Figures are created from simulations computed every 4 seconds. The received signal is computed at every time sample for a constant velocity of 1500m/s in the water layer. The reflection coefficient for each ray takes into account the incidence angle and the nature of the seabed (shale). The model takes into account the fiber response – square cosine of the bearing - and geometrical spreading for amplitude.*

In this section, we have illustrated the DAS capability of recording acoustic waves in underwater environment at both shallow and intermediate depths. We have also demonstrated that it is possible to explain the seemingly complex signal patterns recorded by DAS by taking into account the acoustic wave reverberations and the specific broadside response of the fiber.

We now explore the possibility to record and model the Doppler shift caused by the tanker motion.

V. Doppler estimation

Let's consider a single tonal at frequency f_0 radiated by a ship moving at constant velocity v. For a given receiver R_n, the angle between the boat trajectory and the vector going from the boat to R_n (direct path) is noted φ. This angle is described in 3D using figures 4b and 4c. The instantaneous frequency of the signal received on a given receiver at time *t* is:

$$f(t) = f_0 + \Delta f(t) \tag{3}$$

with:

$$\Delta \boldsymbol{f} = \boldsymbol{f_0}.\boldsymbol{v}.\frac{\boldsymbol{cos\varphi}}{\boldsymbol{c}} \tag{4}$$

where c is the sound speed in the medium and v the velocity of the tanker. Considering a boat moving in a direction perpendicular toward the fiber, as depicted in Figure 4c, φ is minimum when the boat is far away from the fiber and the Doppler frequency shift is maximum. The Doppler frequency shift then decreases when the boat gets closer to the fiber and reaches a minimum value when the boat crosses the fiber. Finally, it increases while the boat travels away from the fiber.

In the case of multipathed rays, and assuming a relatively plane sea bottom, we consider reflections at the bottom and the surface. For multipath 3 and 4 (Figure 4c), with one reflection at the bottom, we call φ' the angle between the boat trajectory and the vector going from the boat to a given receiver R_n. We observe that φ' is closer to 90° than φ. If we consider multipathing with additional surface-bottom reflections, the angle φ' will always increase and get closer to 90°. As a consequence, when ray theory applies and for a relatively plane bottom, the maximum Doppler frequency shift will be reached for the direct path.

Since we performed a f-k analysis on a subset of the DAS array centered on the plumb line of the boat when the boat crosses the fiber (subset 1 in Figure 4a), the emitted signal is seen with positive and negative wavenumbers. We expect, on the one hand, a maximum shift of the Doppler frequency when the boat moves away from the fiber in a direction perpendicular to the fiber (i.e. a k-wavenumber close to zero on subset 1) and, on the other hand, a measured frequency close to the frequency emitted when the boat crosses the fiber, i.e. when the absolute wavenumber reaches its maximum at both ends of subset 1.

At 85m depth, according to Section III, the ship starts to be detected around 49Hz about 850m away from the fiber. At this time and for the closest receiver on the fiber cable R_0 to the axis of the tanker (Figure 4b), we can estimate φ using $tan(\varphi) \approx \frac{85}{850} = 0.1$. This leads to an apparent velocity roughly equal to the tanker velocity for all the receivers in the vicinity of R_0. This also implies that the Doppler variation tends to its maximum possible value $\Delta f = f_0 . \frac{v}{c}$. In the same way, when the 49Hz record ends 5 minutes later, the distance of the fiber is about 850m and the Doppler variation tends to its maximum value but with opposite sign (Figure 4b). Between those two times, considering that the tanker velocity vector is approximatively perpendicular to the fiber, the tanker will cross the fiber with a minimum Doppler variation for the portion of the cable close to R_0.

Using 2D FFT in time and spatial on the recorded DAS data, we represent 8 minute~~s~~-long strain-rate signal - including the 5 minutes 49Hz detection described before - measured along 3km and 5km of fiber in the frequency-wavenumber (f-k) domain when the tanker was passing at 5.8km and 20km offshore respectively (Figure 9). Note that the wavenumber k represented on the x-axis has been divided by 2π so that k = f/c instead of k = ω/c. Then, for any point in the f-k domain, the slope is an estimation of the apparent velocity. When the boat is cruising close to the coast, we observe two ellipses of energy centered around 49.2Hz and 49.4Hz for

$k_x = 0$. These frequencies are shifted by the Doppler effect. Following the interpretation presented above, the two frequencies - 49.2Hz and 49.4Hz around the center of the ellipses - are the ones with minimum Doppler variations, i.e. two frequencies emitted by the tanker that can be recorded vertically above the fiber. For each ellipse, we measure a Doppler shift Δf of about 0.18Hz from the center. Using equation 3, with $f_0 = 49.4$Hz, and $c = 1500$ m/s, it leads to a velocity of 5.5 m/s, which is very close to the 5.6 m/s computed from AIS data. When shifted toward the higher or lower frequencies - the tanker traveling toward or away from the fiber - the wavenumber increases or decreases accordingly, assuming the wave velocity is constant.

At 2000m depth (20km offshore), the f-k processing shows higher energy at two different frequencies and on a narrow range of positive and negative wavenumbers. The two different frequencies are due to two distinct frequencies emitted by the boat around 49.5Hz and are also responsible for the two ellipses observed at shallow depth (Figure 9a). Here, the Doppler shift is less pronounced indicating a slower velocity of the tanker seen by the DAS (Figure 9b). On the abyssal plain, the geometrical spreading is larger, hence a smaller portion of the cable senses the acoustic wave and signals are detected for a small range of angles. Besides, for a given array, the section of the cable receiving signal close to 90° increases with depth, the source being further away. This is the reason why the range of wavenumbers excited is smaller for a boat cruising a deep sea and that null energy around k=0 is more pronounced at greater depth.

The energy peaks around $k = +/- 0.015\ m^{-1}$ come from sections of the cable that detect waves reaching the array with apparent velocity $c = c_0 \cos(\varphi) = f/k = 49.4/0.015 = 3293\ m/s$, according to our convention for k. It therefore corresponds to an angle of 63°, i.e. about 900m from the plumb line of the ship if ray curvature is neglected for this take-off angle. Because the boat crosses the fiber with a nearly perpendicular route around the middle point of the selected portion of the fiber, the same energy is observed traveling landward (positive wavenumber) and seaward (negative wavenumber). The different coherent bands of energy with smaller frequency variations and smaller wavenumbers are related to acoustics waves reflected in the water column. To estimate the Doppler variation, we use an f-k representation of a 1.3 minute-long strain-rate signal (Figure 10). We estimate a maximum shift of 0.12Hz at 49.05 Hz, corresponding to a velocity of 3.7m/s - versus 4.0m/s estimated from AIS positions.

To outline the main features of the f-k representation, we perform a simple modeling of the Doppler variation for a 49.4 Hz source travelling perpendicular to the cable at 5.65 m/s and measured on a 2880 m long cable section at 80 m and then at 2000 m depth. See Figure S2 for the f-k representation of the synthetic signals. Although the model is simple, the main feature of the observed f-k representation are visible on the modeled data: (1) the frequency at the center of the ellipse is equal to the emitted frequency and is the same for all paths, (2) the size of the ellipse decreases as the number of bottom reflections increases and (3) at 2000m depth, only signals with a wavenumber around $k = +/-0.015\ m^{-1}$ reach the fiber.

The f-k representation of underwater DAS records allows us to discriminate environmental signals efficiently from the instrumental noise of the DAS and acquisition system and could be used to detect acoustic signals in a systematic way. Properly modeling of the acoustic propagation in the water column and the Doppler effect, taking into account the bathymetry and the fiber response, we find that it is possible to recover the position of the ship and its noise pattern both at shallow depth and in intermediate water depth.

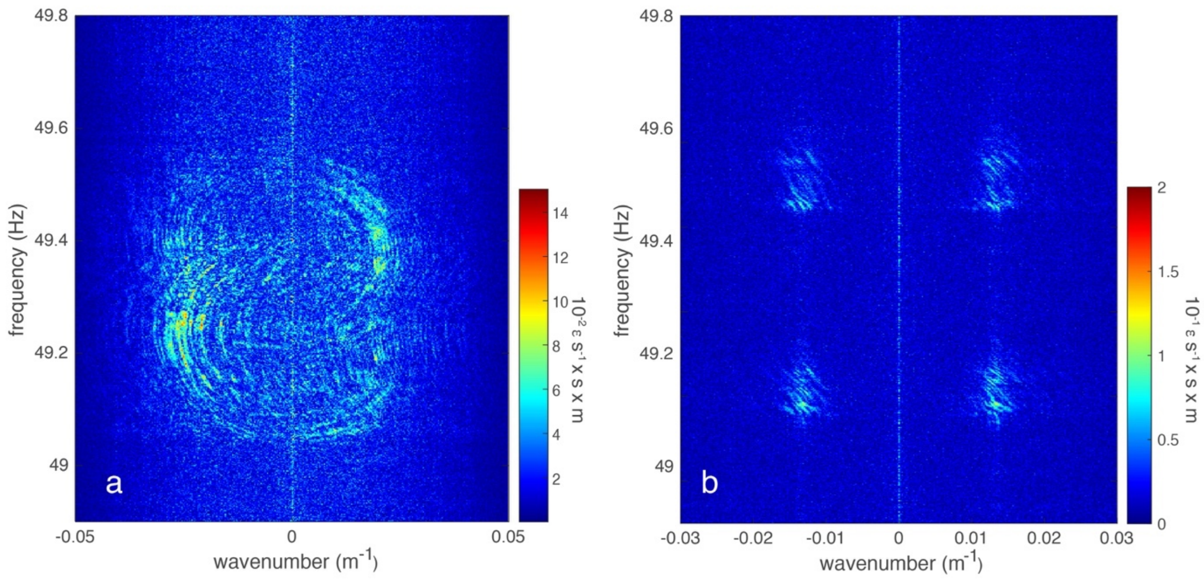

Figure 9 *(color online) Frequency-wavenumber (f-k) decomposition of a 8 minute long strain-rate signal recorded when the tanker is passing above (a) a shallow (85m) section of the cable and (b) a deep section (2000m). The signal is analyzed between 48.9 and 50.1 Hz and decomposed into seaward ($k_x < 0$) and landward ($k_x > 0$) propagating wavefield components. For the shallow section, the signal is averaged between kilometers 4.5 and 7.5 and for the deep section, the signal is averaged between kilometers 17 and 22 of the cable.*

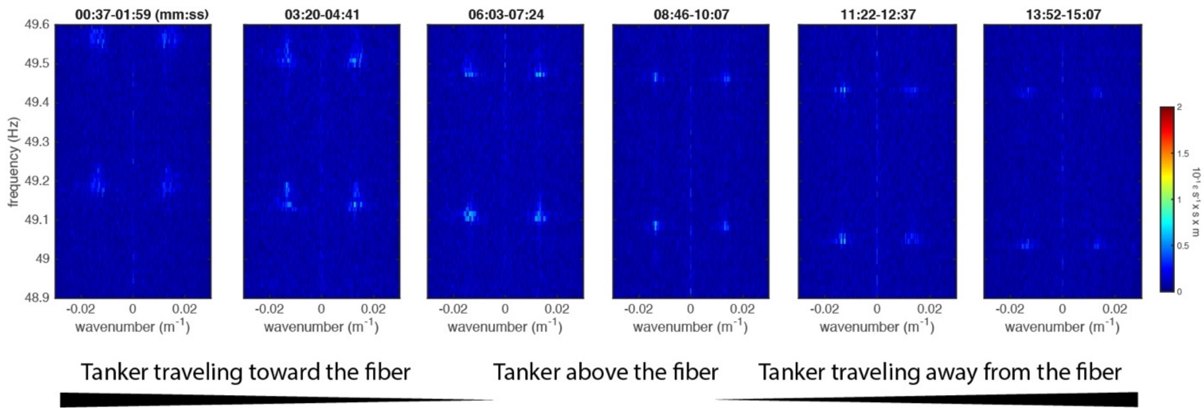

Figure 10 *(color online) Frequency-wavenumber (f-k) decomposition of the strain-rate windowed on a 1.3 ~~minutes~~ long signal between 48.9 and 49.6 Hz, for seaward (k<0) and landward (k>0) components for the 17-22km sections of the fiber when the tanker passed 2000m above the cable.*

VI Assessing the ability to recover the azimuth from a known source

To detect and localize acoustic sources, arrays of sensors use various – and often multidimensional - algorithms such as beamforming, with narrow- or wide-band capabilities. DAS provides arrays of receivers that can be treated as an antenna, to accurately retrieve the azimuth of acoustics sources in the water column. In seismology, beamforming analysis of the DAS signal was successfully used (Lindsey et al. 2017, 2019).

From a linear section of the fiber between 5613m and 5869m, we track the bearing of the tanker using the tonal radiated in the 50Hz frequency band. In theory, a longer array could be used. But, since the cable is not perfectly straight and due to a possible phase shift in the recorded data, we do not investigate longer arrays. We compare the bearing measured through beamforming with a simple synthetic case (Figure 11). For DAS data, the beamforming is computed in the time domain every 5s and the center of the antenna is 59m from the plumb-line from the ship when crossing the fiber according to AIS data. Subset 2 in Figure 4a indicates the position of the selected section of the fiber. In these conditions, the ship is seen approximately at a 90° bearing from the center of subset 2 when the ship is away from the fiber. The ship should deviate from this bearing until she crosses the fiber and then comes back to as she moves away. At 50Hz and for a 256m long antenna, the angular resolution at 3dB is 6°. For the synthetic case, we consider a ship crossing the x-axis at an angle of 85° and a speed of 11 knots. With the channel at a depth of 80 m, we assume that the main source of noise radiated by the boat is 65 m above the seafloor. We compute the bearing angle of the ship from a point on the x-axis 60 m away of the point where the ship crosses the x-axis. Figure 11, we observe close agreement between the measured points (red triangles) and the simulated data (blue line). As expected, when the ship gets closer to the fiber, we observe a deviation from the initial bearing of 90°,-between roughly 60 and 100 s before returning to it in a similar way.

Considering a water column of 85m, we estimate that the boat crossed the fiber at a distance of 5821m from the coast, whereas the real distance is closer to 5800m according to the AIS positioning. This difference, which is about the width of the tanker, could be linked to depth approximation or AIS bias. Besides, model used for the beamforming supposes a perfect alignment of the receiver, which is not proven. By reducing the array length to 128m, the impact of a potential curvature of the fiber is reduced and the newfound position becomes 5806m instead of 5800m.

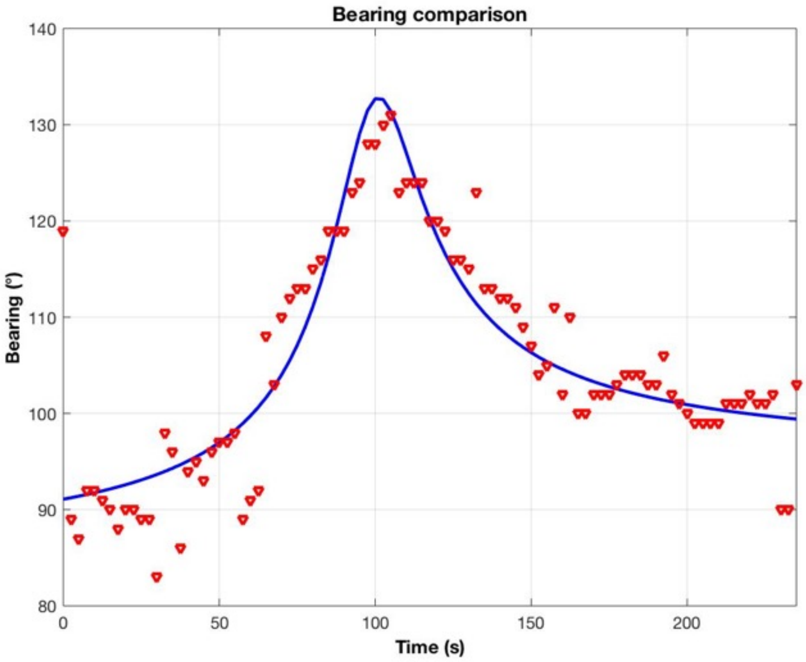

Figure 11 *(color online) Bearing measurements performed using beamforming over a linear antenna of 256m length and centered at 5741m from the fiber extremity, i.e. 59m away of the point where the ship crosses the fiber (red) compared with the theoretical bearing computed for a point 60m away from the point where the ship crosses the fiber 65m above the seafloor (blue). The beamforming is performed every 5 seconds using the recorded signal filtered in the [48, 51] Hz band.*

Discussion

Our analysis demonstrates that it is possible to perform continuous and distributed monitoring of acoustic noise sources over several tens of kilometers using DAS and seafloor optical fiber cables. Acoustic waves traveling in the water layer interact directly with the fiber or penetrate the subsurface in case the cable is slightly buried in the sediments.

We detect and track a tanker in water up to 2000 m deep from the acoustic waves it produces. The appearance of frequency narrow bands in the time-frequency spectrum, over a given distance, and at a given time, and a Doppler shift of the frequency with time are the characteristics of the noise emitted by a ship and are therefore quite easy to distinguish from environmental and DAS self-noise.

We model the principal features of the tanker acoustic signal using an analytical model. First-order features like the ring shape interference pattern and its energy decay right below the boat are well explained by the model, acknowledging reflections of the acoustic waves in the water column, and the DAS broadside sensitivity. However, for more accurate modeling of the intensity of the acoustic field in time and space, numerical models taking into account the wavefront curvature, the full system response, the Doppler effect, the impedance of the sediments, and a non-constant water velocity profile should be used. Modeling of noise emitted by ships could also help to estimate the coupling of the cable with the ground, a critical step to calibrate the response of the cable and study non-anthropogenic signals - earthquakes, landslide, acoustic waves. More detailed analyses would probably require experiments with calibrated instruments, such as hydrophones.

Beamforming takes advantage of the distributed sensing capability of DAS to allow precise positioning of maritime vessels both in time and space. The example given in section VI shows the impact of fiber positioning. Additional calibration (using e.g. calibrated sources) to better estimate the fiber response and position should also improve the result of the algorithm. Future beamforms should also integrate this azimuthal response of the fiber. The acoustic noise of vessels cruising in deeper waters needs to be further explored. The attenuation of the acoustic wave with depth strongly depends on the celerity profile of the sea, and therefore could limit the range of depth in which we can detect signals with frequency higher than 100Hz. Few existing fiber-optic cables can provide some insight about the feasibility to measure acoustic noise at depth larger than 2000m because the repeaters limit the DAS sensing range to 30-50km in general. However, on the first 30-50 km of cable the depth is rarely deeper that 2000m, and it already offers a remarkable coverage.

We demonstrate the reliability of measuring accurately high-frequency signal (up to 100Hz) on a telecom cable, which allows exploring other sources of acoustic signals in addition to seismic waves. The noise mapping that we presented confirms the multidisciplinary potential for DAS on seafloor cables.

Conclusion

We demonstrate the feasibility to record noise emitted by a boat at both shallow (85m) and in the deep sea (2000m) using DAS on a standard underwater telecom cable and we confirmed our inferences by comparison with AIS data. Using f-k representation, it is possible to discriminate between moving sources, static sources and noise, and to assess the speed of the moving sources by measuring the Doppler shift. Monitoring anthropogenic noise over a wide range of depths can help the scientific community to estimate its impact on marine life. Also, DAS telecom cables are very long underwater antennas - tens of kilometers - and very dense - every meter - that can serve to retrieve precisely the azimuth of noise sources, such as maritime vessels. If equipped with repeaters allowing the back-scattered light to reach the DAS interrogator, worldwide telecom cables can serve as distributed environmental sensors measuring anthropogenic and environmental noise and maritime traffic.

Acknowledgements

This work was supported by the SEAFOOD project, funded in part by grant ANR-17-CE04-0007 of the French Agence Nationale de la Recherche and in part by Université Côte d'Azur IDEX program UCA JEDI ANR-15-IDEX-0001. We thank the Centre de Physique des Particules de Marseille who facilitated the access the infrastructure. The MEUST infrastructure is financed with the support of the CNRS/IN2P3, the Region Sud, France (CPER), the State (DRRT) and the Europe (FEDER).

APPENDIX

Appendix A : DAS sensitivity to an incident acoustic waves on the fiber optic.

Acoustic-waves that propagate in an 3D infinite homogenous fluid medium are pressure fluctuations that can be modeled by the linear wave equation as described in (Kinsler et al. 1999)

$$\nabla^2 p - \frac{1}{c^2}\frac{\partial^2 p}{\partial t} = 0 \qquad \text{(A1)}$$

with p the acoustic pressure at a given position defined by the vector position $\vec{r}$ =(x,y,z), ∇^2 the Laplace operator and c the acoustic wave velocity. We can express this acoustic-wave in terms of a particle velocity $\boldsymbol{v}$ that is also governed by the linear wave equation.

$$\nabla^2 \boldsymbol{v} - \frac{1}{c^2}\frac{\partial^2 \boldsymbol{v}}{\partial t} = 0 \qquad \text{(A2)}$$

Considering a monochromatic plane wave travelling in a direction defined by the wave vector $\overrightarrow{k}$, the solution of equation (A2) is given by

$$v = A_v \hat{e}_k e^{i(\omega t - \vec{k}.\vec{r})} \quad \text{(A3)}$$

with ω the pulsation, and $\hat{e}_k = \frac{\vec{k}}{\|\vec{k}\|}$ the unit vector in the direction of propagation with k the wavenumber and A_v the amplitude of the planar wavefield of the particle velocity in the direction of propagation.

Taking the x-axis of the coordinate system colinear to the fiber optic cable, the wave vector $\vec{k}$ forms an angle θ with the x-axis (also called the bearing angle). The projection of $\boldsymbol{v}$ along the x-axis is

$$v_x = A_v cos\theta e^{i(\omega t - \vec{k}.\vec{r})} \quad \text{(A4)}$$

The resulting strain ε_{xx} which is a change in length Δl per unit of the original length l produced along the fiber is given by

$$\varepsilon_{xx} = \frac{\partial u_x}{\partial x} \quad \text{(A5)}$$

The particle velocity being the time derivative of the displacement, the displacement vector is given by $u_x = \frac{1}{i\omega} v_x$. We then expresses the strain as a function of the particle velocity,

$$\varepsilon_{xx} = \frac{-k_x}{\omega} v_x, \text{ where } k_x = kcos\theta$$

$$\frac{-kA_v}{\omega} cos^2\theta e^{i(\omega t - \vec{k}.\vec{r})}, c = \frac{\omega}{k}$$

$$\frac{-A_v}{c} cos^2\theta e^{i(\omega t - \vec{k}.\vec{r})} \quad \text{(A6)}$$

As shown in equation (A6), for acoustic waves, the measured strain along the x-axis shows a square cosine dependency on the bearing angle. This dependency is the same for elastic P-waves (Mateeva et al. 2014).

In DAS sensing, the strain along the fiber is measured over a gauge-length L. The underlying principles of DAS sensing are reported in Masoudi & Newson (2016), Daley et al. (2016) and Jousset et al. (2017). Following Bakku (2015), the expression of ε_{xx}^{DAS} is given by

$$\varepsilon_{xx}^{DAS} = \int_{z-\frac{L}{2}}^{z+\frac{L}{2}} \frac{\varepsilon_{xx}}{L} dx' = \frac{-A_v}{c} cos^2\theta e^{i(\omega t - k_y y - k_z z)} \int_{z-\frac{L}{2}}^{z+\frac{L}{2}} e^{-ik_x x'} dx'$$

$$\frac{A_v}{cL} cos^2\theta \frac{e^{i(\omega t - k_y y - k_z z)}}{ik_x} \left[e^{-ik_x x'}\right]_{x-\frac{L}{2}}^{x+\frac{L}{2}}$$

$$\frac{A_v}{cL} cos^2\theta \frac{e^{i(\omega t - k_y y - k_z z)}}{ik_x} e^{-ik_x x} \left(-2isin\left(\frac{k_x L}{2}\right)\right)$$

$$\frac{-A_v}{c} cos^2\theta e^{i(\omega t - k_x x - k_y y - ik_z z)} \frac{sin\left(\frac{k_x L}{2}\right)}{\frac{k_x L}{2}}$$

$$\varepsilon_{xx}^{DAS} = \varepsilon_{xx} \mathrm{sinc}\left(\frac{k_x L}{2}\right) \qquad \text{(A7)}$$

Equation A7 shows a sinc dependency on gauge length L of the strain measured using DAS. For a DAS that measures strain-rate, i.e. change in strain with respect to time, the sinc dependency still holds

$$\dot{\varepsilon}_{xx}^{DAS} = \dot{\varepsilon}_{xx} \mathrm{sinc}\left(\frac{k_x L}{2}\right). \qquad \text{(A8)}$$

Appendix B : Modeling of acoustic signals measured using DAS

The synthetic data are simulated using ray theory. For each receiver at time t_r, the emitted time t_e and the distance traveled r are computed using 2nd order equation using a constant velocity. We neglect attenuation and assume that the amplitude is only influenced by geometrical spreading and possibly reflection coefficients. The DAS square cosine response is applied with regard to the bearing angle θ considering a fiber along the x-axis and the sinc dependency with gauge length L is added.

Then, for an emitted signal at frequency f_0 we get:

$$u(t_r) = \frac{1}{r} cos^2\theta sinc\left(\frac{k_x \mathrm{L}}{2}\right) sin\,(2\pi f t_e)$$

with $k_x = 2\pi f cos\,\theta / c$

In addition, for multipathed signals, two coefficients are added:

- -1.0 in the case of surface reflection
- Fresnel coefficient $\left|\frac{Z_2 cos\theta_2 - Z_1 cos\theta_1}{Z_2 cos\theta_2 + Z_1 cos\theta_1}\right|$ in case of bottom reflection, θ_1 and θ_2 being respectively the incidence angle and the transmitted angle and Z_1 and Z_2 the acoustic impedance of the water and of the first bottom layer. The impedance is equals to the density times the P wave velocity $\mathrm{Z} = \rho V_P$. For the bottom layer impedance we used a V_P value of 4400m/s and a density of 2500 kg/m^3 for the shale (Mascle 1971).

References

Ajo-Franklin, J.B., Dou, S., Lindsey, N.J., Monga, I., Tracy, C., Robertson, M., Rodriguez-Tribaldos, V., Ulrich, C., Freifeld, B., Daley, T., Li, X. (2019). Distributed Acoustic Sensing Using Dark Fiber for Near-Surface Characterization and Broadband Seismic Event Detection. *Sci Rep* **9,** 1328 (2019). https://doi.org/10.1038/s41598-018-36675-8

Bakku, S. K. (2015). Fracture characterization from seismic measurements in a borehole (Doctoral dissertation, Massachusetts Institute of Technology).

Coyle,P. KM3NeT Collaboration (2017). KM3NeT-ORCA: Oscillation Research with Cosmics in the Abyss. J. Phys. Conf. Ser. 888 , 012024. https://dx.doi.org/10.1088/1742-6596/888/1/012024

Daley, T. M., Freifeld, B. M., Ajo-Franklin, J., Dou, S., Pevzner, R., Shulakova, V., Kashikar, S., Miller, D.E., Goetz, J., Henninges, J., Lueth, S. (2013). Field testing of fiber-optic distributed acoustic sensing (DAS) for subsurface seismic monitoring. *The Leading Edge*, *32*, 936–942. https://doi.org/10.1190/tle32060699.1

Daley, T., Miller, D. E., Dodds, K., Cook, P. & Freifield, B. M. Field testing of modular borehole monitoring with simultaneous acoustic sensing and geophone vertical seismic profiles at Citronelle, Alabama. Geophys. Prospect. 12,1318–1334 (2016). https://doi.org/10.1111/1365-2478.12324

Dou, S., Lindsey, N. J., Wagner, A., Daley, T. M., Freifeld, B. M., Robertson, M., Peterson, J., Ulrich, C., Martin, E., Ajo-Franklin, J. B. (2017). Distributed acoustic sensing for seismic monitoring of the near surface: A traffic-noise interferometry case study. *Scientific Reports*, *7*(1), 11620. doi: 10.1038/s41598-017-11986-4.

Etter, P. C. (2018). *Underwater acoustic modeling and simulation 5th edition*. CRC press, Boca Raton, FL).

Etter, P. C. "New frontiers for underwater acoustic modeling," *2012 Oceans*, Hampton Roads, VA, 2012, pp. 1-10, doi: 10.1109/OCEANS.2012.6404775.

Favali, P., & Beranzoli, L. (2009). EMSO: European multidisciplinary seafloor observatory. Nuclear Instruments and Methods in Physics Research Section A: Accelerators, Spectrometers, Detectors and Associated Equipment, 602(1), 21-27. doi:10.1016/j.nima.2008.12.214

Feigl, K. L., Parker, L. M., & Team, P. (2019). PoroTomo Final Technical Report: Poroelastic Tomography by Adjoint Inverse Modeling of Data from Seismology, Geodesy, and Hydrology (No. 3.1). University of Wisconsin System. https://doi.org/10.2172/1499141

Fournier, G. (2009). Hydroacoustique et bruit des navires. *Techniques de l'ingénieur. Bruit et vibrations*, (BR2030).

Frisk, G. V. (2012). Noiseonomics: The relationship between ambient noise levels in the sea and global economic trends. Scientific reports, 2, 437 https://doi.org/10.1038/srep00437

Gray, L. M., & Greeley, D. S. (1980). Source level model for propeller blade rate radiation for the world's merchant fleet. *the Journal of the Acoustical Society of America*, *67*(2), 516-522. https://doi.org/10.1121/1.383916

Hello, Y.; Royer, J.Y.; Rivet, D.; Charvis, P.; Yegikyan, M.; Philippe, "New versatile autonomous platforms for long-term geophysical monitoring in the ocean," *OCEANS 2019 - Marseille*, Marseille, France, 2019, pp. 1-8, doi: 10.1109/OCEANSE.2019.8867216.

Hermannsen, L., Mikkelsen, L., Tougaard, J., Beedholm, K., Johnson, M., & Madsen, P. T. (2019). Recreational vessels without Automatic Identification System (AIS) dominate anthropogenic noise contributions to a shallow water soundscape. *Sci Rep* **9,** 15477. https://doi.org/10.1038/s41598-019-51222-9

Jousset, P., Reinsch, T., Ryberg, T., Blanck, H., Clarke, A., Aghayev, R., Hersis, G.P., Henninges, J., Weber, M. and Krawczyk, C. M. (2018). Dynamic strain determination using fiber-optic cables allows imaging of seismological and structural features. *Nat Commun* **9,** 2509. https://doi.org/10.1038/s41467-018-04860-y

Kinsler, L. E., Frey, A. R., Coppens, A. B., & Sanders, J. V. (1999). Fundamentals of acoustics 4th Edition, John Wiley and Sons Inc., Hoboken.

P. Lamare, The MEUST deep sea infrastructure in the Toulon site. EPJ Web Conf. 1 16, 09001 (2016).

Lellouch, A., Horne, S., Meadows, M. A., Farris, S., Nemeth, T., & Biondi, B. (2019). DAS observations and modeling of perforation-induced guided waves in a shale reservoir. *The Leading Edge*, *38*(11), 858-864. https://doi.org/10.1190/tle38110858.1

Lindsey N. J., Martin, E.R., Dreger D.S., Freifeld B., Cole S., James S.R., Biondi B.L. and Jonathan B. Ajo-Franklin, J.B. (2017) Fiber-Optic Network Observations of Earthquake Wavefields. Geophysical Research Letters. 11792-11799. https://doi.org/10.1002/2017GL075722

Lindsey, N. J., Dawe, T. C., & Ajo-Franklin, J. B. (2019). Illuminating seafloor faults and ocean dynamics with dark fiber distributed acoustic sensing. Science, 366(6469), 1103-1107. DOI: 10.1126/science.aay5881

Mascle, J. (1971). Géologie sous-marine du canyon de Toulon. Cahiers Océanographiques, 23, 241-250. Open Access version : https://archimer.ifremer.fr/doc/00000/4890/

Masoudi, A. & Newson, T. P. Contributed review: distributed optical fibre dynamic strain sensing. Rev. Sci. Instrum. 87, 011501 (2016). https://doi.org/10.1063/1.4939482

Mateeva, A., Lopez, J., Mestayer, J., Wills, P., Cox, B., Kiyashchenko, D., Yang, Z., Berlang, W., Detomo, R. and Grandi, S. (2013). Distributed acoustic sensing for reservoir monitoring with VSP. *The Leading Edge*, *32*, 1278–1283. https://doi.org/10.1190/tle32101278.1

Mateeva, A., Lopez, J., Potters, H., Mestayer, J., Cox, B., Kiyashchenko, D., Wills, P., Grandi, S., Hornman, K., Kuvshinov, B., Berlang, W., Yang, Z. and Detomo, R. (2014). Distributed acoustic sensing for reservoir monitoring with vertical seismic profiling. Geophysical Prospecting, 62(4), 679-692. https://doi.org/10.1111/1365-2478.12116

McKenna, M., Ross D., Wiggins S. and Hildebrand J. (2012). Underwater radiated noise from modern commercial ships. *The Journal of the Acoustical Society of America*, *131*(1), 92-103. https://doi.org/10.1121/1.3664100

McKenna, M., Wiggins, S. & Hildebrand, J. Relationship between container ship underwater noise levels and ship design, operational and oceanographic conditions. Sci Rep 3, 1760 (2013). https://doi.org/10.1038/srep01760

Merchant, N. D. (2019). Underwater noise abatement: Economic factors and policy options. Environmental science & policy, 92, 116-123. https://doi.org/10.1016/j.envsci.2018.11.014

Miller, D. E., Daley, T. M., White, D., Freifeld, B. M., Robertson, M., Cocker, J., & Craven, M. (2016). Simultaneous acquisition of distributed acoustic sensing VSP with multi-mode and single-mode fiber-optic cables and 3-component geophones at the Aquistore CO_2 storage site. CSEG Recorder: June 2016, 28.

Mustonen M., Klauson A., Folégot T. and Clorennec D. (2020). Natural sound estimation in shallow water near shipping lane. *The Journal of the Acoustical Society of America*, *147*(2), EL177-EL183. https://doi.org/10.1121/10.0000749

Nishimura, C. E. and Conlon, D. M. (1994) IUSS dual use: Monitoring of whales and earthquakes using SOSUS, Mar. Technol. Soc. J., 1994, vol. 27, no. 4

Pillon, D. (2016). Introduction à la détection sous-marine passive, Techniques de l'ingénieur, *Bruit et vibrations*, (RAD6712)

Rønnekleiv, E., Brenne, J. K., Waagaard, O. H., Moussakhani B. (2019) Distributed acoustic sensing for submarine cable protection. Suboptic2019, 8-11 April 2019 - New Orleans Marriott - 555 Canal Street, New Orleans, Louisiana 70130 USA.

S. Salon, A. Crise, P. Picco, E. de Marinis, O. Gasparini. Sound speed in the Mediterranean Sea: an analysis from a climatological data set. *Annales Geophysicae*, European Geosciences Union, 2003, 21 (3), pp.833-846. https://doi.org/10.5194/angeo-21-833-2003

Sladen, A., Rivet, D., Ampuero, J. P., De Barros, L., Hello, Y., Calbris, G., and Lamare, P. (2019). Distributed sensing of earthquakes and ocean-solid Earth interactions on seafloor telecom cables. *Nature Communications*, *10*(1), 1-8. https://doi.org/10.1038/s41467-019-13793-z

Turgut, A., Orr, M., & Rouseff, D. (2010). Broadband source localization using horizontal-beam acoustic intensity striations. The Journal of the Acoustical Society of America, 127(1), 73-83. doi: 10.1121/1.3257211.

M. Vespe, I. Visentini, K. Bryan, and P. Braca, "Unsupervised learning of maritime traffic patterns for anomaly detection," in Proc. 9th IET Data Fusion Target Tracking Conf., Algorithms Appl., 2012, pp. 1–5. doi: 10.1109/ICNC.2015.7378165.

Wales S.C. and Heitmeyer R.M., 2002. An ensemble source spectra model for merchantship-radiated noise. . J. Acoust. Soc. Am.111(3). https://doi.org/10.1121/1.1427355

Wales S.C. and Heitmeyer R.M., 2011. Merchant ship-radiated noise source levels. J. Acoust. Soc. Am. 129(4) doi: 10.1121/1.3587657

Williams, E., Fernandez-Ruiz, M. R., Magalhaes, R., Vanthillo, R., Zhan, Z., Gonzalez-Herraez, M., & Martins, H. F. (2019). Teleseisms and Microseisms on an Ocean-Bottom Distributed Acoustic Sensing Array. https://doi.org/10.31223/osf.io/kg7q4

Wiggins, S. M., and Hildebrand, J. A. (2007). "High-frequency Acoustic Recording Package (HARP) for broad-band, long-term marine mammal monitoring.," (IEEE, Tokyo, Japan, International Symposium on Underwater Technology and Workshop on Scientific Use of Submarine Cables and Related Technologies), pp. 551-557.

Williams, R., Wright, A.J., Ashe, E., Blight, L.K., Bruintjes, R., Canessa, R., Clark, C.W.,Cullis-Suzuki, S., Dakin, D.T., Erbe, C., Hammond, P.S., Merchant, N.D., O'Hara, P.D.,Purser, J., Radford, A.N., Simpson, S.D., Thomas, L., Wale, M.A., (2015). Impacts of anthropogenic noise on marine life: publication patterns, new discoveries, and future directions in research and management. Ocean Coast. Manag. 115, 17–24. https://doi.org/10.1016/j.ocecoaman.2015.05.021.

Yu, Chunquan, Zhongwen Zhan, Nathaniel J. Lindsey, Jonathan B. Ajo-Franklin, and Michelle Robertson (2019). The Potential of DAS in Teleseismic Studies: Insights From the Goldstone Experiment. Geophysical Research Letters 46 (3): 1320–28. https://doi.org/10.1029/2018GL081195.

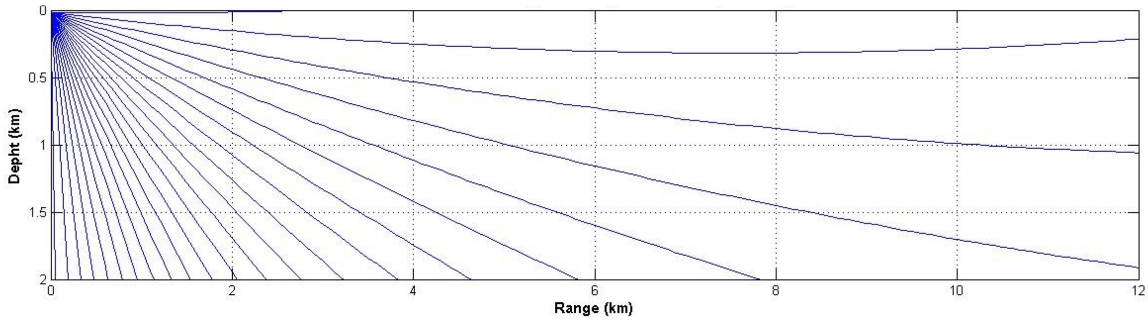

Figure *S1 Reflection in a constant gradient g=0.01ms*$^{-1}$ *for a source located at 15m depth.*

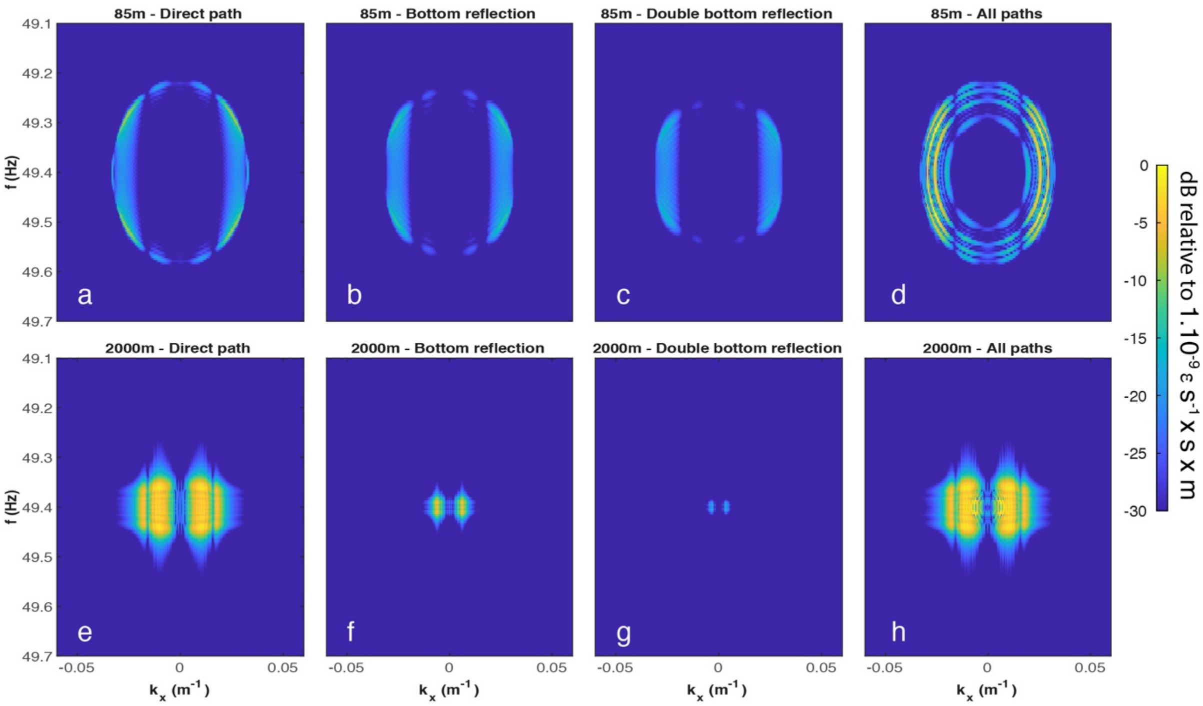

Figure S2 *f-k representation of synthetic signal emitted by a moving source at 49.4 Hz travelling perpendicular to the cable at 5.56 m/s and recorded by a 2880 m long array, for a 85m channel depth (top) and a 2000m channel depth (bottom). The direct ray path (a,e), the path with a single bottom reflection (b,f), the path with two bottom reflexion (c,g) are modeled individually, then the first eight acoustic rays are modeled (d,h).*